Supporting Information

Water-based synthesis of chemically stable Zr-based MOFs using pyridine-containing ligands and their exceptionally high adsorption capacity for iodine

Zhe Wang, Ying Huang, Jian Yang, Yongsheng Li, Qixin Zhuang and Jinlou Gu*

Key Laboratory for Ultrafine Materials of Ministry of Education, School of Materials Science and Engineering, East China University of Science and Technology, Shanghai 200237, China

Fax: +86-21-64250740; Tel: +86-21-64252599

Email: jinlougu@ecust.edu.cn

Table S1. Summary of the compositions for hydrothermal synthesis of UiO-66-PYDC MOFs.[a]

$ZrCl_4$ (g)	PYDC (g)	HAc (mL)	H_2O (mL)	HAc/ H_2O (molar ratio)
0.233	0.168	0	10	0
0.233	0.168	2	8	1:12.5
0.233	0.168	4	6	1:5
0.233	0.168	6	4	1:2.17
0.233	0.168	8	2	1:0.8
0.233	0.168	10	0	Pure HAc

[a] The systematic investigation of the chemical reaction system was carried out in a 20 mL screw glass bottle. To optimize the reaction conditions, the HAc/H_2O ratio was optimized in the experiments. The optimized reaction condition is highlighted by grey background. For all syntheses, the reaction time was set to 24 h and the reaction temperature was adjusted to 100 °C.

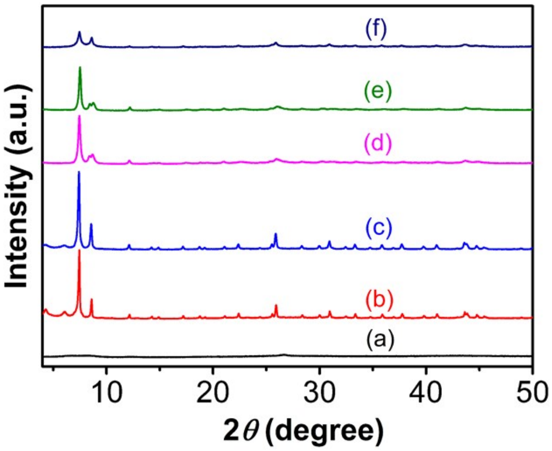

Fig. S1. PXRD patterns of the products synthesized at different feed ratio of HAc/H_2O from (a) 0, (b) 1:12.5, (c) 1:5, (d) 1:2.17, (e) 1:0.8, and (f) Pure HAc.

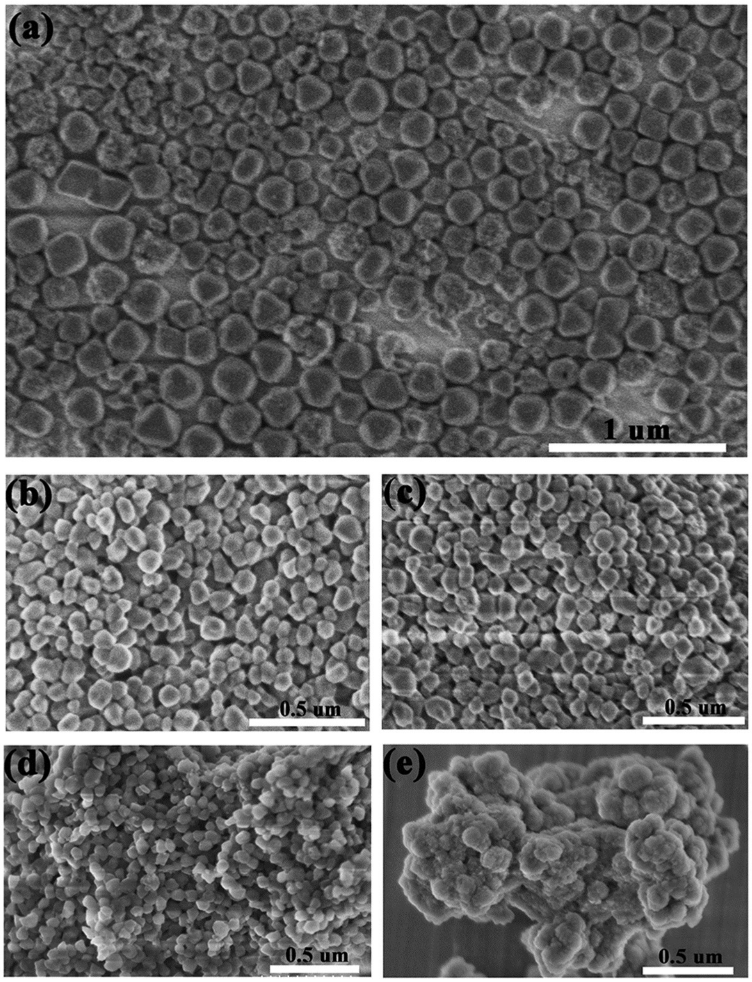

Fig. S2. FE-SEM images of UiO-66-PYDC MOFs obtained at different feed ratio of HAc/H_2O from (a) 1:12.5, (b) 1:5, (c) 1:2.17, (d) 1:0.8, and (e) Pure HAc.

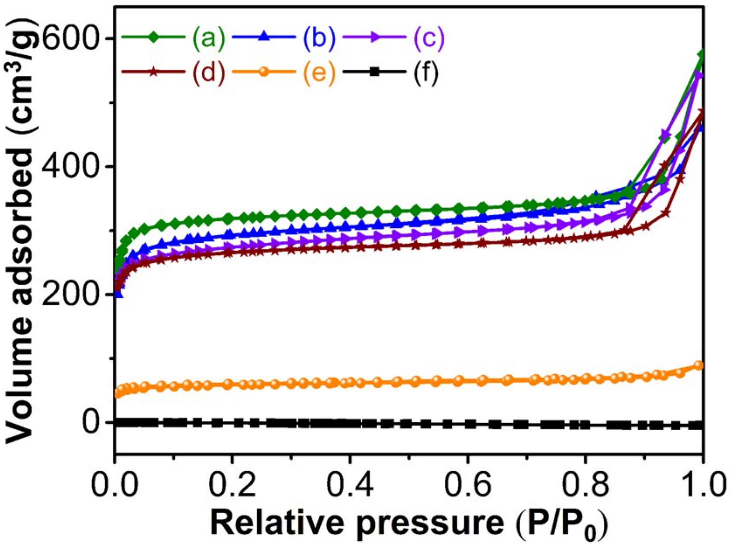

Fig. S3. Nitrogen adsorption-desorption isotherms of the samples synthesized at different feed ratio of HAc/H_2O from (a) 1:5, (b) 1:12.5, (c) 1:2.17, (d) 1:0.8, (e) Pure HAc, and (f) 0.

Table S2. Texture parameters of the MOF samples synthesized using different amount of HAc.

Samples	**S_{BET} (m^2/g)**	**V_p (cm^3/g)**
UiO-66-PYDC-0	0	0
UiO-66-PYDC-1:12.5	953	0.35
UiO-66-PYDC-1:5	1030	0.43
UiO-66-PYDC-1:2.17	859	0.35
UiO-66-PYDC-1:0.8	648	0.32
UiO-66-PYDC-Pure HAc	190	0.07

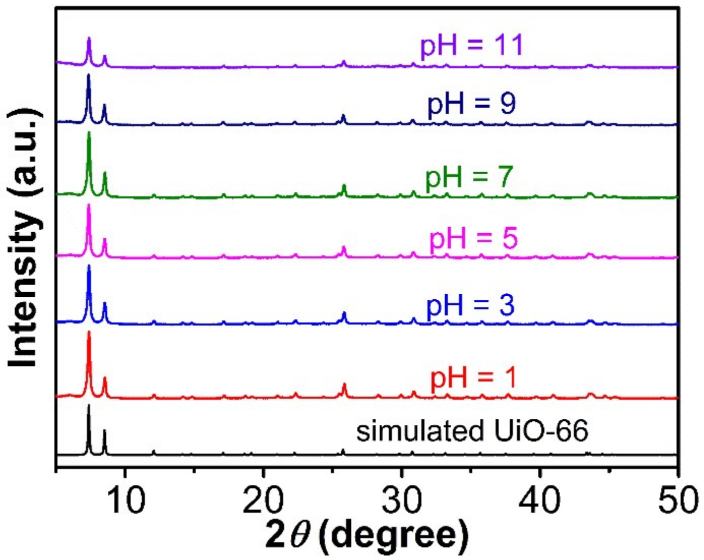

Fig. S4. XRD patterns for UiO-66-PYDC synthesized with HAc/H_2O ratio of 1:5, and the samples were soaked in aqueous solutions with various pH values of 1, 3, 5, 7, 9, and 11 for 24 h.

Table S3. Specific surface areas and pore volumes of UiO-66-PYDC MOFs after their soaking in aqueous solutions with different pH values.

Samples	**S_{BET} (m^2/g)**	**V_p (cm^3/g)**
UiO-66-PYDC-pH=1	860	0.34
UiO-66-PYDC-pH=3	908	0.36
UiO-66-PYDC-pH=5	932	0.35
UiO-66-PYDC-pH=7	903	0.34
UiO-66-PYDC-pH=9	881	0.31
UiO-66-PYDC-pH=11	809	0.29

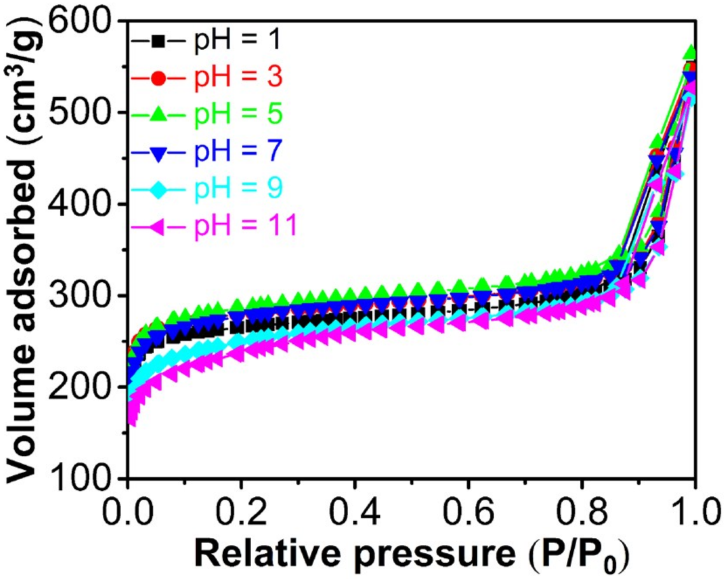

Fig. S5. Nitrogen adsorption-desorption isotherms of UiO-66-PYDC synthesized with HAc/H_2O ratio of 1:5 and the samples were soaked in aqueous solutions with various pH values of 1, 3, 5, 7, 9, and 11 for 24 h.

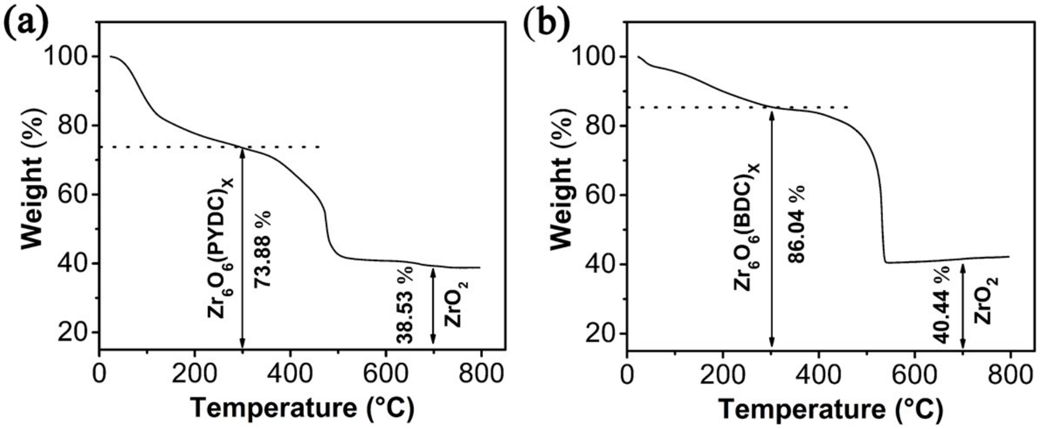

Fig. S6. Thermogravimetric analysis (TGA) curves of (a) UiO-66-PYDC and (b) UiO-66.

To further understand the adsorption kinetics of I_2 over samples, the pseudo-first-order (Equation 1) and pseudo-second-order (Equation 2) were employed to fit experimental data.

$$\log(q_e - q_t) = \log q_e - \frac{k_1}{2.303}t \qquad \textbf{(S1)}$$

$$\frac{t}{q_t} = \frac{1}{k_2 q_e^{\ 2}} + \frac{t}{q_e} \qquad \textbf{(S2)}$$

where q_e (mg g^{-1}) and q_t (mg g^{-1}) are the amounts of I_2 adsorbed at equilibrium and at time t (h), respectively; t (h) is adsorption time and k_2 (g mg^{-1} h^{-1}) is the pseudo-second-order adsorption rate constant. k_2 can be calculated from the slope and intercept of plot t/q_t versus t.

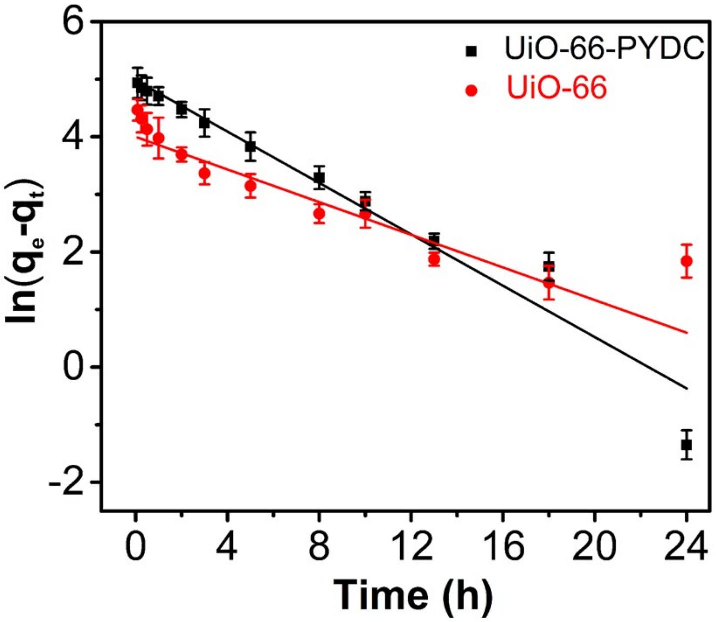

Fig. S7. Pseudo-first-order kinetics of I_2 removal on UiO-66-PYDC (black), and UiO-66 (red) (T = 25 °C, $C_{initial}$ = 127 mg L^{-1}).

The Langmuir model is presented as the following equation (3):

$$\frac{C_e}{q_e} = \frac{1}{k_L q_{\max}} + \frac{C_e}{q_{\max}} \qquad \textbf{(S3)}$$

where C_e (mg/L) is the concentration of I_2 under equilibrium condition, q_e represents the adsorption capacity of I_2 at equilibrium status (mg/g), k_L is the Langmuir constant (L/mg) concerning adsorption energy and affinity of binding sites, and q_{max} is the maximum adsorption capacity (mg/g).

Freundlich adsorption equation (4) has the linear form as following:

$$\log q_e = \log k_F + (n)\log C_e \qquad \textbf{(S4)}$$

k_F (mg^{1-n} L^n/g) is Freundlich constant related to the adsorption capacity of the adsorbent and n denotes heterogeneity factor. The value of n reflects the type of isotherm to be favorable ($0<n<1$), irreversible ($n=0$) or unfavorable ($n>1$).

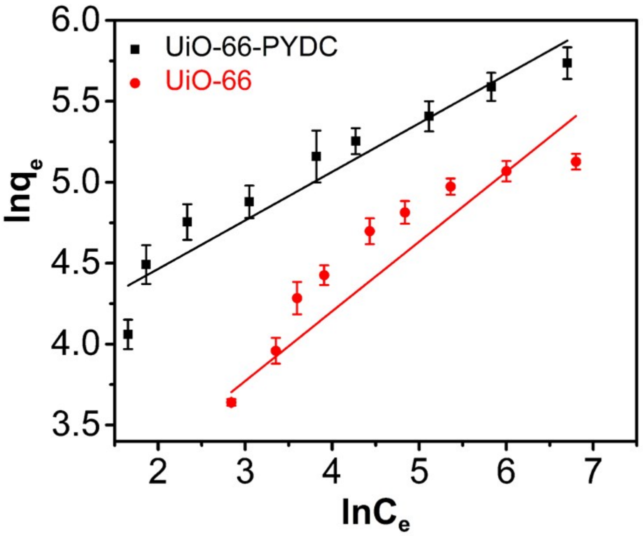

Fig. S8. Freundlich model of the uptake of I_2 over UiO-66-PYDC (black), and UiO-66 (red) (T = 25 °C, $C_{adsorbent}$ = 600 mg L^{-1}).

Table S4. Comparison of I_2 adsorption capacities onto various MOFs.

Adsorbents	**q_{max} (mg/g)**	**References**
MIL-101-NH_2	311	46
TMU-16-NH_2	450	23
NiP-CMP	326	29
$[Co^{II}_3(lac)_2(pybz)_2]$	900	15
$[Zn_3(DL\text{-}lac)_2(pybz)_2]_n$	1000	47
UiO-66-PYDC	1250	this work

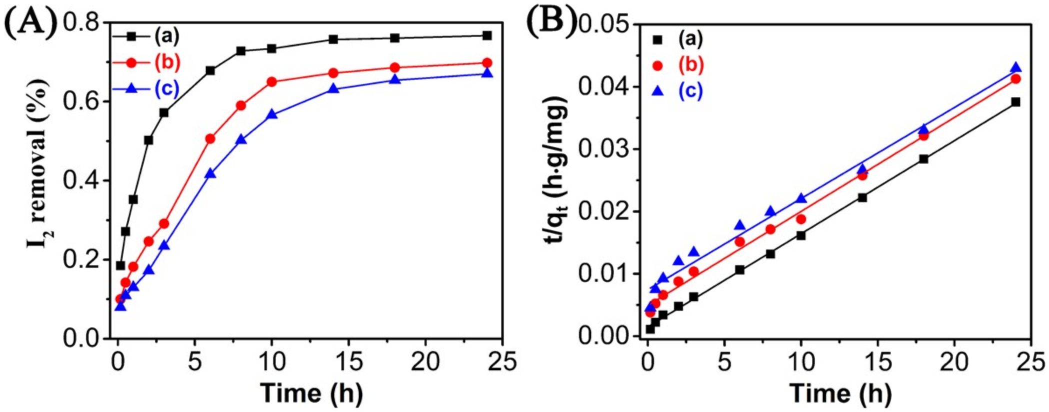

Fig. S9. (A) Kinetic profiles of I_2 adsorption cycle onto UiO-66-PYDC, (a) cycle 1, (b) cycle 2, and (c) cycle 3 in cyclohexane solution, and (B) the corresponding plots of pseudo-second-order kinetic of I_2 adsorption cycle onto UiO-66-PYDC (a) cycle 1, (b) cycle 2, and (c) cycle 3 (T = 25°C, $C_{inital} = 500$ mg L^{-1}).

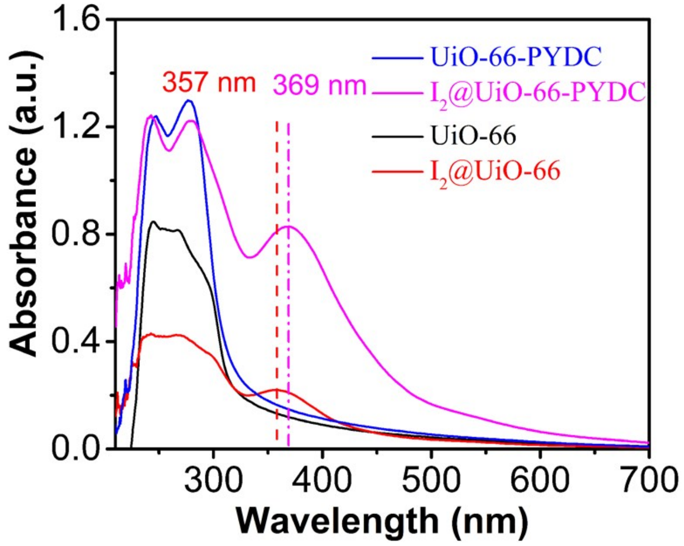

Fig. S10. UV-vis spectra of UiO-66-PYDC (blue), I_2@UiO-66-PYDC (carmine), UiO-66 (black), and I_2@UiO-66 (red).

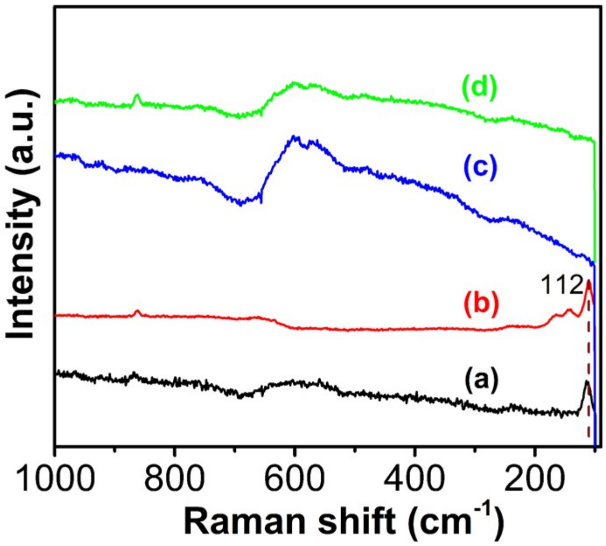

Fig. S11. Raman spectra of (a) I_2@UiO-66-PYDC, (b) I_2@UiO-66, (c) UiO-66-PYDC, and (d) UiO-66.

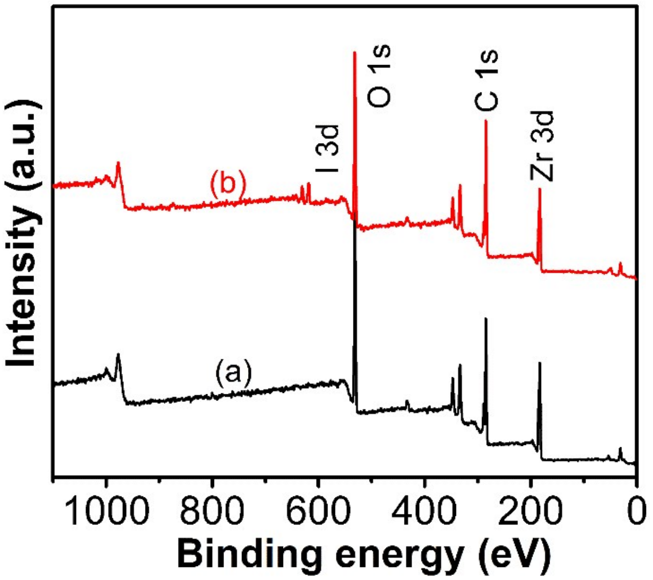

Fig. S12. Wide scan XPS spectra of (a) UiO-66-PYDC, and (b) I_2@UiO-66-PYDC.

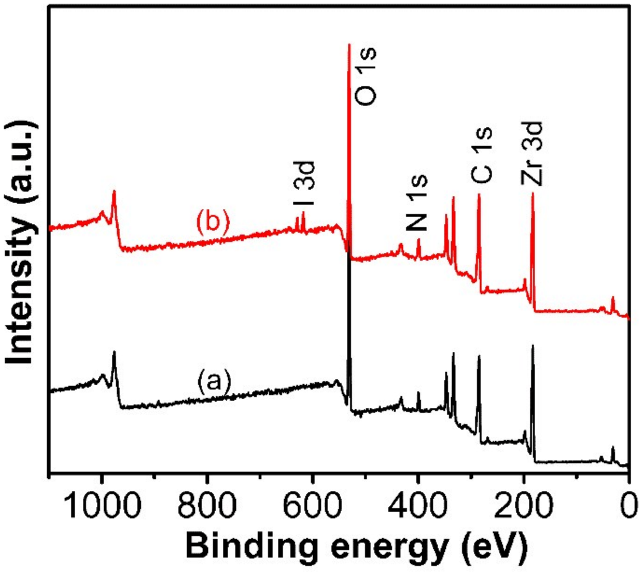

Fig. S13. Wide scan XPS spectra of (a) UiO-66, and (b) I_2@UiO-66.

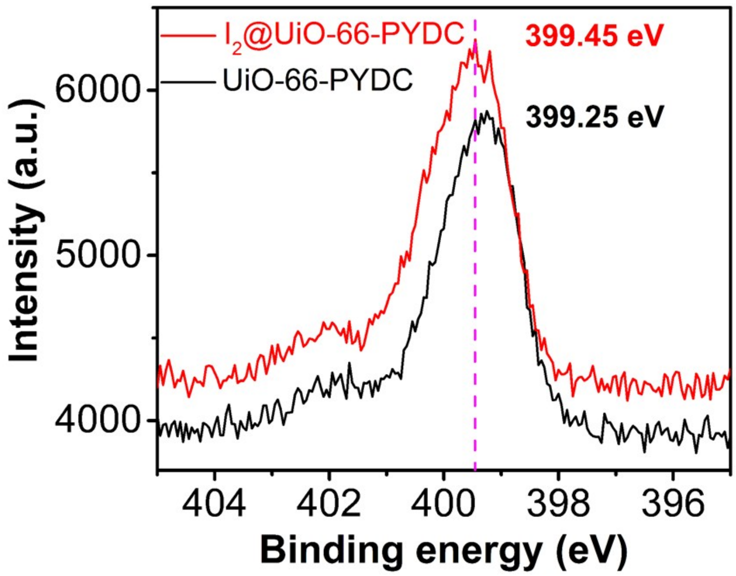

Fig. S14. The high resolution XPS spectra of N 1s recorded for I_2@UiO-66-PYDC (red) and UiO-66-PYDC (black).